An investigation of the influence of 3d printing defects on the tensile performance of ABS material

Materials Today: Proceedings

An investigation of the influence of 3d printing defects on the tensile performance of ABS material

--Manuscript Draft--

Manuscript Number:	
Article Type:	SI:ICAMSE2022
Keywords:	3d printing; ABS; porosity; X-ray tomography; tensile performance; digital image correlation
Corresponding Author:	Serena Rifuggiato, M.D. Politecnico di Torino Torino, ITALY
First Author:	Serena Rifuggiato, M.D.
Order of Authors:	Serena Rifuggiato, M.D.
	Paolo Minetola, Associate Professor
	Vito Stiuso, Research fellow
	Mankirat Singh Khandpur, Ph.D. Student
	Luca Fontana, Ph.D. Student
	Luca Iuliano, Full professor
Abstract:	Recently, the popularity of 3d printing for industrial and consumer use has spread across many different sectors. For this reason, quality assurance of 3d printed parts is becoming increasingly important. The extrusion and layer-by-layer deposition of a polymer filament on the print bed can introduce defects such as pores and voids into the internal structure of 3d printed parts. The relation between 3d printing defects and tensile performance of 3d printed samples is studied in this paper. The study considers tensile specimens of acrylonitrile butadiene styrene (ABS) that were 3d printed by varying the infill strategy and percentage to simulate different levels of strength for the part. Before the tensile tests, the ABS samples were inspected by X-ray tomography to identify the presence of internal voids generated by the 3d printing process. For each sample, data and statistics about the internal defects were used for determining a relation with the tensile test results. The local deformation of the sample and the position of the final fracture were observed using a digital camera and digital image correlation (DIC). In most cases, the experimental results confirmed the matching between the presence of internal voids and the areas of high deformation. However, the position of the specimen fracture did not always coincide with the largest defects. Nevertheless, this study highlights the importance of non-destructive inspection in quality assurance of 3d printed parts when in-situ monitoring of the 3d printing process is not applied.

Available online at www.sciencedirect.com

ScienceDirect

materialstoday: PROCEEDINGS

[Name of the proceedings]

An investigation of the influence of 3d printing defects on the tensile performance of ABS material

Serena Rifuggiato*, Paolo Minetola, Vito Stiuso, Mankirat Singh Khandpur, Luca Fontana, Luca Iuliano

Politecnico di Torino, Department of Management and Production Engineering (DIGEP), Corso Duca degli Abruzzi 24, 10129 Torino, Italy

Abstract

Recently, the popularity of 3d printing for industrial and consumer use has spread across many different sectors. For this reason, quality assurance of 3d printed parts is becoming increasingly important. The extrusion and layer-by-layer deposition of a polymer filament on the print bed can introduce defects such as pores and voids into the internal structure of 3d printed parts. The relation between 3d printing defects and tensile performance of 3d printed samples is studied in this paper. The study considers tensile specimens of acrylonitrile butadiene styrene (ABS) that were 3d printed by varying the infill strategy and percentage to simulate different levels of strength for the part. Before the tensile tests, the ABS samples were inspected by X-ray tomography to identify the presence of internal voids generated by the 3d printing process. For each sample, data and statistics about the internal defects were used for determining a relation with the tensile test results. The local deformation of the sample and the position of the final fracture were observed using a digital camera and digital image correlation (DIC). In most cases, the experimental results confirmed the matching between the presence of internal voids and the areas of high deformation. However, the position of the specimen fracture did not always coincide with the largest defects. Nevertheless, this study highlights the importance of non-destructive inspection in quality assurance of 3d printed parts when in-situ monitoring of the 3d printing process is not applied.

Keywords: 3d printing; ABS; porosity; X-ray tomography; tensile performance; digital image correlation.

1. Introduction

Additive Manufacturing (AM), initially known as Rapid Prototyping, refers to a group of layerwise manufacturing techniques that allow to easily create objects with high complex geometries directly starting from a 3d CAD model imported in the slicing software of the AM machine [1]. Nowadays, Additive Manufacturing is not only adopted for prototyping, but also to produce end-usable parts using different materials (metals, polymers, composites, and ceramics) and techniques.

As concerns AM for polymers, 3d printing is one of the most popular techniques. The 3d printing process is also known as Fused Deposition Modelling (FDM) or Fused Filament Fabrication (FFF) [2]. This additive process is based on the selective deposition of a heated and extruded thermoplastic filament on a build platform layer after layer. The nature of the process is mainly a thermal one and the viscoelastic flow of the extruded polymeric filament can introduce some heterogeneities such as pores and air bubbles whose position, shape and dimension are not predictable. However, these kinds of flaws might compromise the structural integrity of the part [3, 4]. Some studies, through a design of experiment (DOE) approach, showed that process parameters like the number of layers, the hatch distance, the build orientation, air gap, raster width and infill strategy have a deep influence on the porosity of the part, affecting the

* Corresponding author. Tel.: +39-011-090-7295; fax: +39-011-090-7299.
E-mail address: serena.rifuggiato@polito.it

resulting mechanical properties [5-8]. Therefore, the characterization of these defects could improve the fabrication process itself because they strongly depend on the process parameters.

This work is aimed at finding a relation between the presence of large pores and the tensile strength of 3d printed parts of acrylonitrile butadiene styrene (ABS) material. For this reason, tensile specimens are assumed as the reference geometry for the study. The size of the largest voids generated during 3d printing is investigated for different infill strategies and percentages, that are assumed as the main process parameters of the deposition of the thermoplastic filament within one layer of the part.

To detect the presence of internal defects in the 3d printed specimens, a suitable non-destructive testing (NDT) method should be used for investigating the inner structure of the part, without the need to destroy it when in-situ process monitoring is not applicable [9]. Among NDT methods, X-ray computed tomography (CT-scan) is considered the most flexible and efficient technique for AM components [10-12].

Therefore, the 3d printed tensile specimens were inspected by X-ray CT before the tensile test. A digital camera was used during the testing phase to monitor the local deformation of the specimens by the digital image correlation (DIC) method [13]. The information of porosities extracted by the CT-scan data is then combined with the DIC analysis for the identification of a cause-effect relationship between the presence of internal voids and the failure of the specimens. A detailed description of the experimental procedures is provided in the following section. The third section of the paper is focused on the analysis of the experimental data, and the conclusions are presented in the end.

2. Materials and methods

2.1. Specimen fabrication

The geometry of tensile samples for the experimental campaign was designed with reference to the Type I specimen of the ASTM D638 standard [14]. In the most restricted area, the Type I specimen (Figure 1a) has a nominal width of 13 mm in one 3d printing layer, which is a suitable size to adopt different infill percentages and strategies for the deposition of the extruded filament.

The specimens were fabricated using a yellow ABS filament supplied by Filoalfa with a 2.85 mm diameter. The filament was loaded in a 3d printer model A4v3 by 3ntr. The printing parameters and the deposition path (Fig. 1 b) of the tensile specimens were set in KisSlicer software. Different infill percentages (25%, 50%, and 100%) and different infill strategies (octagonal and straight) were selected as reported in Table 1. 100% infill percentage can be set for the straight strategy only in KisSlicer. Except for the infill percentage and strategy, all the other process parameters were left unchanged to their default value for the ABS material: layer thickness of 0.2 mm, bed temperature of 120 °C and nozzle temperature of 255 °C. From the combination of the parameters in Table 1, five different ISO g-code were generated by KisSlicer software. The numerical control g-code files were then loaded into Repetier-Host software and sent one at a time to the A4v3 printer for manufacturing several replicas of the samples. Two copies were fabricated for specimens A and C, while three replicas were printed for specimens B and D and four copies for specimen E.

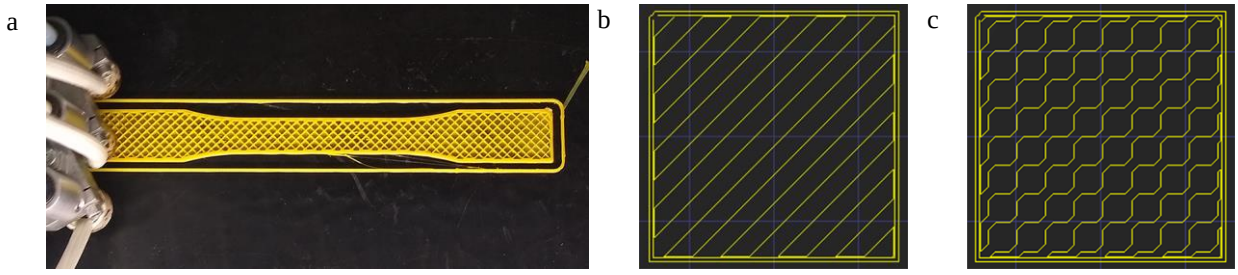

Fig. 1. 3d printing of a C specimen (a); 25% straight infill path (b) and 25% octagonal infill path (c).

2.2. X-ray inspection

Computed tomography is an optical non-destructive technology based on the emission of X radiations to gather information on the material distribution inside a part. For this study, a micro-CT scan model Phoenix v|tome|x S240 by GE Baker Hughes (Fig. 2a) was used together with the on-board datos|acquisition® software to inspect the 3d printed replicas of the tensile specimens (Fig. 2b).

Table 1. Process parameters applied to print tensile test specimens

Test specimen	Infill strategy	Infill percentage	Width (mm)	Thickness (mm)
A_1	Octagonal	25%	13.54	2.85
A_2	Octagonal	25%	13.20	2.91
B_1	Octagonal	50%	13.58	3.04
B_2	Octagonal	50%	13.45	3.10
B_3	Octagonal	50%	13.42	3.00
C_1	Straight	25%	13.31	2.87
C_2	Straight	25%	13.39	2.84
D_1	Straight	50%	13.47	2.93
D_2	Straight	50%	13.53	2.93
D_3	Straight	50%	13.30	2.88
E_1	Straight	100%	13.40	3.16
E_2	Straight	100%	13.50	3.10
E_3	Straight	100%	13.25	2.99
E_4	Straight	100%	13.22	3.04

a b

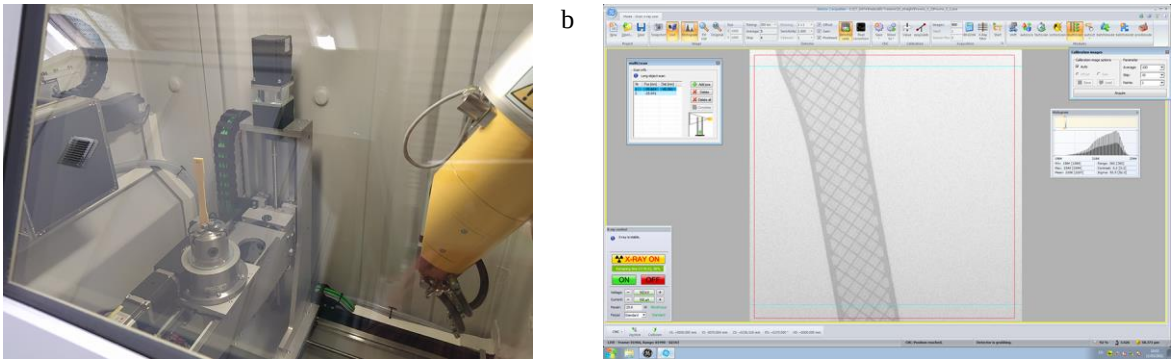

Fig. 2. Working volume of the CT-scan v|tome|x S240 (a); tomographic image for C_2 specimen in datos|acquisition (b).

To reduce the inspection time, only the portion of the specimen corresponding to the most restricted cross-section with a width of 13 mm was scanned, since the fracture during tensile testing should occur in this region. Therefore, the area of interest for NDT inspection includes the whole straight central part of the tensile specimen and the beginning of the fillets of the dogbone geometry. The X-ray scans were carried out with a resolution of 58.37 µm (voxel size), which was obtained by placing every specimen at a distance of 236.52 mm from the X-ray source. In this configuration, two scans are needed to complete the inspection of the area of interest of one specimen by using the multi-scan function of datos|acquisition software. For each scan, between 800 and 1000 images were acquired during the rotation of the specimen depending on its inclination and orientation with respect to the detector panel. To correctly penetrate the ABS material with adequate power, a voltage of 160 kV and a current of 160 µA were set for the X-ray source. The scanning settings are summarized in Table 2.

Table 2. Scanning settings values

Voltage *(kV)*	Current *(µA)*	Timing *(ms)*	Skip	Average	Images	Voxel size *(µm)*
160	160	200	4	3	800-900-1000	58.37

The first 4 images were skipped after each rotation increment to avoid wrong data acquisition and distorted images due to vibrations, while the average is considered for the data values acquired over the next 3 images for each angular position of the sample. Under these conditions, the multi-scan process is completed in about 40 minutes for each tensile specimen.

At the end of the scanning, the reconstruction of the 3d data from the set of X-ray images captured by the CT-scan panel was carried out by means of datos|reconstruction® software. After the acquisition and reconstruction phases, the 3d scan data was imported into VG Studio Max software (version 3.4) by Volume Graphics for visualization and analysis of voxel data. Before starting the porosity analysis, data segmentation or surface determination is needed.

Segmentation determines the respective interfaces between solid materials and surrounding air or between different solid materials converting 3d voxel data into 3d surface data. The technique used by VG Studio Max software involves assigning a threshold grey value to edge voxels. Based on the results of surface reconstruction, the porosity/inclusion analysis module of the software runs the automatic and fast detection of material discontinuities, such as pores and inclusions. In this study, the efficient defect detection algorithm VGDefX® was applied for the identification of voilds inside the 3d printed tensile specimens of ABS material. The result of the computation consisted of a report providing various characteristics for each pore (defect position, defect sphericity/compactness, defect size, etc.) and statistical information, such as the overall percentage of porosity in the part.

After NDT inspection of each specimen, the tensile test was carried out using an AURA 10T machine by Easydur. An external USB camera model SV-USBFHD06H-SFV by Svpro (Fig. 3a) was used to apply the optical strain measurement technique of digital image correlation (DIC). The Svpro camera has a Sony IMX322 sensor whose resolution is 2 Megapixels (1920 x 1080 pixels). Before testing, the surface of the specimens was prepared for the optical acquisition by spraying a speckle pattern of acrylic blue paint over the yellow ABS material (Fig. 3b).

The image correlation algorithm computes the local strain of the specimen by identification of the position of the same points into two consecutive images of the surface, that are extracted as frames of the video recorded by the USB camera during the test. This correlation is achieved by dividing the surface of interest into square subsets or facets of pixels detected by the DIC software thanks to the creation of the speckles pattern on the specimen surface.

Therefore, after preparation of the surface, every tensile test was recorded by the digital camera and the video frames were then imported into GOM Correlate software for DIC analysis (Fig. 4). During the test, the load and displacement data were also recorded using the EasyQS software of the tensile machine.

For the purpose of this study, only the ultimate tensile strength (UTS) value is considered among the tensile properties of each 3d printed specimen together with the size of the three largest voids and the porosity content resulting from the analysis of the CT data. The position of these main flaws was also compared to the one of the area of major local deformation detected by the DIC analysis to investigate the influence of major 3d printing pores on the resistance of the samples.

a b

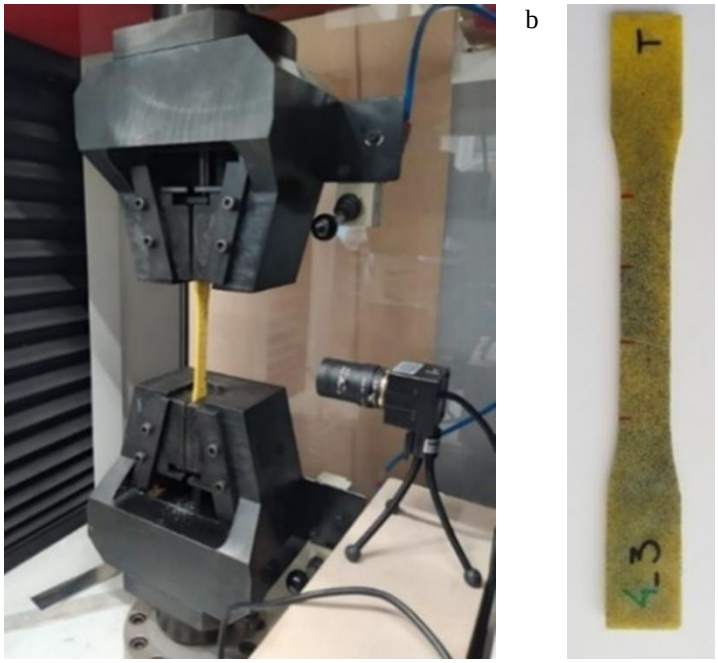

Fig. 3. Tensile test configuration with the digital camera for DIC (a) and preparation of the specimen surface (b).

a b

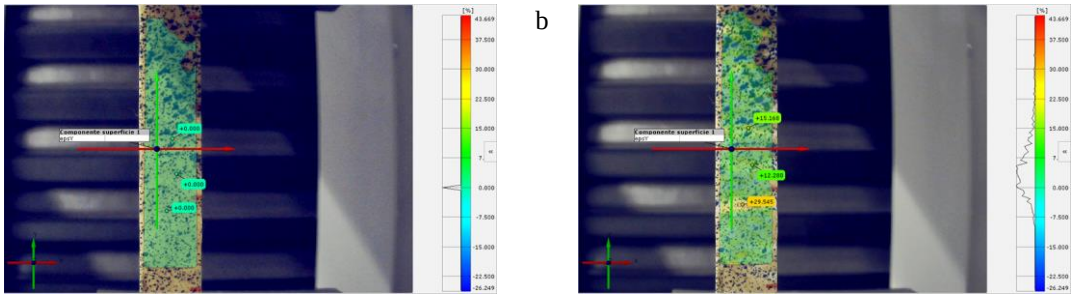

Fig. 4. Local deformation values resulting from DIC analysis at (a) 0 seconds (a) and 26 seconds (b) for B_1 sample.

3. Experimental results

3.1. Porosity analysis from CT data

For each specimen, only the first largest voids resulting from the porosity analysis of CT scan data were considered, since it was assumed that these main flaws could affect the tensile strength the most. The volume of these pores is reported in Table 3, while a comparison of the porosity percentage of the whole specimen is proposed in Fig. 5.

Table 3. Volumes of the three main largest voids of each tensile specimen.

Test specimen	Infill	Volume of primary void (mm^3)	Volume of secondary void (mm^3)	Volume of tertiary void (mm^3)
A_1	25% octagonal	0.49	0.38	0.17
A_2	25% octagonal	0.40	0.34	0.13
B_1	50% octagonal	0.10	0.06	0.06
B_2	50% octagonal	0.09	0.08	0.08
B_3	50% octagonal	0.06	0.06	0.05
C_1	25% straight	0.12	0.06	0.06
C_2	25% straight	0.17	0.07	0.06
D_1	50% straight	0.28	0.25	0.21
D_2	50% straight	0.27	0.21	0.21
D_3	50% straight	0.18	0.17	0.17
E_1	100% straight	0.05	0.02	0.01
E_2	100% straight	0.02	0.02	0.02
E_3	100% straight	0.09	0.07	0.07
E_4	100% straight	0.12	0.10	0.06

For the specimens printed with octagonal strategy, larger pores were identified in the case of 25% infill (A specimens) if compared to 50% infill (B specimens). On the contrary, in the case of the straight infill strategy, the samples with 50% infill (D specimens) had larger voids than the specimens with 25% infill (C specimens).

The smallest volume of the main pores was measured for two out of four specimens with 100% infill (E specimens).

For each type of infill strategy, specimens with 50% infill were characterized by a greater porosity percentage than specimens with 25% infill. This result can be explained by the major amount of material in the first ones.

When compared to specimens with 50% octagonal infill (B specimens), tensile samples with 50% straight infill (D specimens) presented a smaller percentage of porosity. Higher porosity percentages were measured in three out of four specimens with 100% straight infill (E specimens). Although the three main voids for E specimens have smaller sizes than the pores in other specimens (Table 3), more material is deposited for 100% infill and the resulting porosity percentage is higher. Specimen E_1 constitutes an exception because it has a very low porosity percentage, which is even lower than that of samples with 25% infill. These samples (A and C specimens) have a similar porosity percentage around 0.5 % for both orthogonal and straight infill.

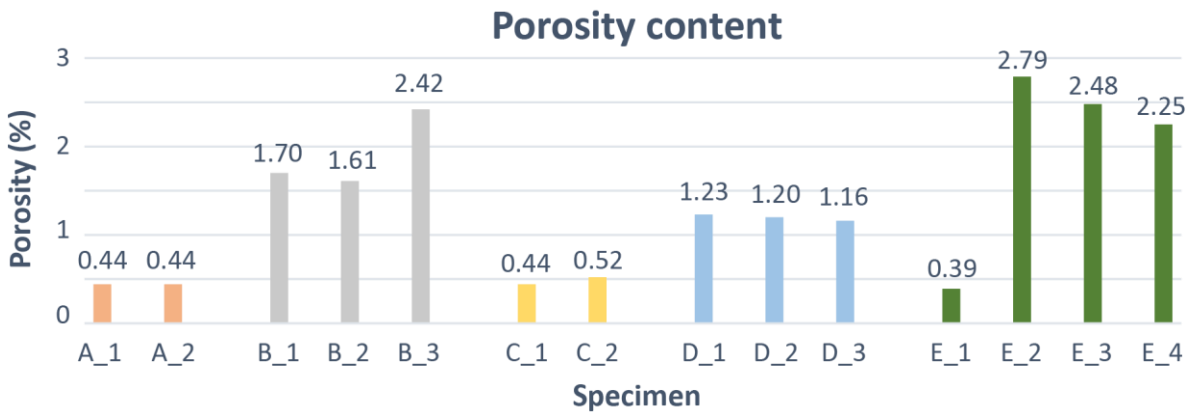

Fig. 5. Porosity content resulting from CT data of each ABS specimen.

3.2. Tensile test results

The load-displacement curves traced using the values recorded by the EasyQS software of the Aura10T machine are shown in Fig. 6 for all the specimens. Moreover, the software provided the value (Fig. 7) of the ultimate tensile stress (UTS) that was computed as the maximum load divided by the initial value of the restricted cross-section, whose main dimensions are included in Table 1 for each specimen.

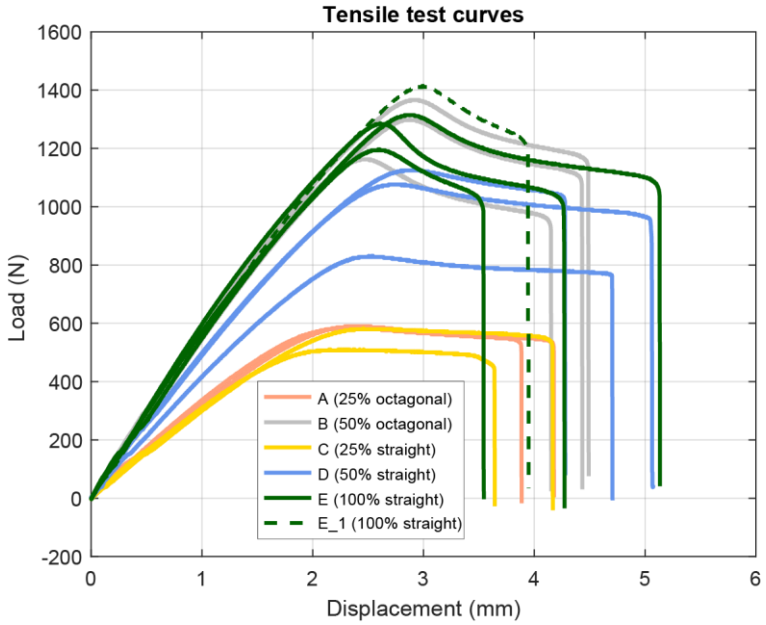

Fig. 6. Tensile curves resulting from the tests of the 3d printed ABS samples.

First of all, as it could be expected, it was observed that specimens with 25% infill, corresponding to less material in the cross-sections and build layers, withstood a lower maximum load than the samples with higher infill percentages. The UTS of the A and C specimens with an infill of 25% was around 15 MPa for both infill strategies. However, there was a difference of about 5 MPa between the two C specimens. Sample C_1 with a lower porosity (0.44 %) content demonstrated a higher tensile strength than the C_2 specimen with higher porosity (0.52%). This result suggests a relation between the mechanical strength and the porosity content, which is also confirmed by the A specimens. These samples, that had the same porosity percentage (0.44 %), could withstand the same tensile load. In addition, among E specimens, sample E_1 with the lowest porosity percentage had the highest tensile strength.

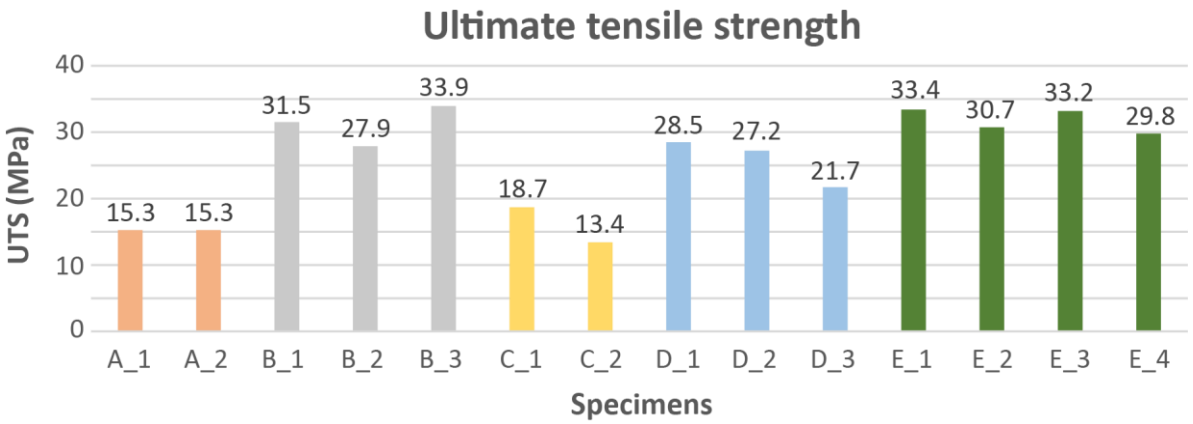

Fig. 7. UTS values of each 3d printed ABS specimen.

Conversely, in the other specimens with 50% or 100% of infill percentage, the relation between the UTS and the porosity content could not be clearly distinguished. For example, the porosity content in D specimens with 50% straight infill was lower than that of B specimens with 50% octagonal infill. Thus, the tensile strength of D samples should have been higher than the one of B samples, whereas it resulted in a slightly lower average value. It might be concluded that the difference in the porosity content among most of the specimens with 50% and 100% infill is not large enough to significantly determine a corresponding variation in the UTS of the 3d printed ABS material.

3.3. Matching between voids locations and the most stressed areas

CT scan data was aligned with the results of the DIC analysis to search for a match between the position of the main voids in Table 3 and the location of the regions where the fracture or a high deformation occurred during tensile testing.

To this aim, the 3d CAD model of the tensile specimen was imported in GOM Correlate software and was used as the reference for alignment of the DIC results together with the 3d CT data. By visual comparison of the aligned data and using the point-to-point distance measuring function of the software, the distance between the closest pore to the most stressed region and to the final fracture location was evaluated for every specimen.

Table 4. Voids closed to the region of the specimen fracture and to the band of major deformation.

Test specimen	Infill	Closest void to the fracture region *(volume in mm^3)*	Distance from the fracture region	Closest void to the major deformation band *(volume in mm^3)*	Distance from the major deformation band
A_1	25% octagonal	Tertiary *(0.17)*	17.9 mm	Tertiary *(0.17)*	6.6 mm
A_2	25% octagonal	Tertiary *(0.13)*	17.8 mm	Tertiary *(0.13)*	7.1 mm
B_1	50% octagonal	Tertiary *(0.06)*	1.3 mm	Secondary *(0.06)*	2.8 mm
B_2	50% octagonal	Primary *(0.09)*	30.8 mm	Secondary *(0.08)*	14 mm
B_3	50% octagonal	Secondary *(0.06)*	16.8 mm	Secondary *(0.06)*	2.0 mm
C_1	25% straight	Tertiary *(0.06)*	1.9 mm	Secondary *(0.06)*	0.2 mm
C_2	25% straight	Secondary *(0.07)*	27.7 mm	Secondary *(0.07)*	1.8 mm
D_1	50% straight	Tertiary *(0.07)*	4.0 mm	Primary *(0.28)*	2.1 mm
D_2	50% straight	Tertiary *(0.07)*	0.2 mm	Primary *(0.27)*	0.1 mm
D_3	50% straight	Primary *(0.18)*	20.1 mm	Tertiary *(0.17)*	0.8 mm
E_1	100% straight	Secondary *(0.02)*	18.2 mm	Tertiary *(0.01)*	0.7 mm
E_2	100% straight	Primary *(0.02)*	2.2 mm	Primary *(0.02)*	5.0 mm
E_3	100% straight	Secondary *(0.07)*	11.8 mm	Secondary *(0.07)*	4.0 mm
E_4	100% straight	Primary *(0.10)*	0.9 mm	Secondary *(0.1)*	1.4 mm

A correction was needed to consider that the pore position in the 3d scan data was evaluated in the unstressed specimen, whereas DIC data accounts for the progressive real strain of the material during the tensile test. To account for this difference, the elongation of a specimen was evaluated by means of four equally spaced marks that were placed with a red marker in the central portion of the specimen surface (Fig. 3b) before testing. The real position of the three main voids was then corrected considering the elongation and finally, the distance to the most critical zones was measured. Measurement results are summarized in Table 4 for the void with the shortest distance in each specimen.

With reference to the pore position, the evolution of local strain was monitored through the DIC software. By observing all the phases of every tensile test, it was noticed that for some specimens, the material started straining at the site of one or more voids. However, after a few seconds, the strain increased in another location where the specimen then failed at the end of the test. This result could indicate an initial influence of the considered void on the specimen, but the presence of the void became then negligible because the specimen broke or deformed more in other zones. This behaviour might suggest that, during the test, the coalescence of smaller voids in a larger pore assumed more importance for the failure than the initial major flaw. An example is shown in Fig.8, wherein the blue line represents the evolution of the strain at the position of one of the main voids, while the black curve represents the strain at the point where the specimen failed.

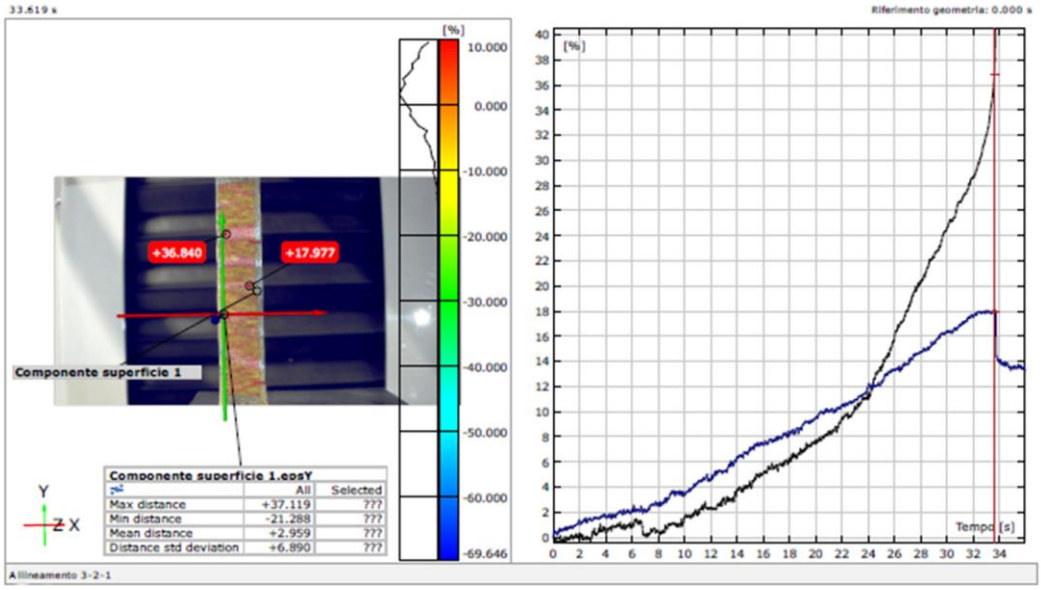

Fig.8. Evolution of tensile strain at two points in specimen B_3.

It was observed that in all the specimens with 25% infill (specimens A and C) the position of the main voids occurred at the interface between the inner infill path and the outer wall of the samples (Fig. 9 and Fig. 10). This result highlights the repeatability of the 3d printing process and can be explained by considering the deposition and distribution of the 3d printed filament, which is concentrated along the specimen border in the case of lower infill percentages.

a

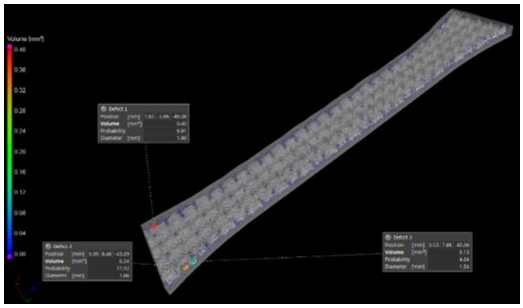

b

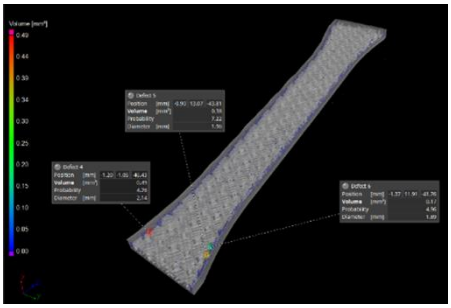

Fig. 9. Similar position of the main voids in specimen A_1 (a) and specimen A_2 (b).

In the A specimens, the areas of fracture or largest deformation were not close to the three main flaws. Nevertheless, as a peculiar aspect, it could be noticed that the tree main voids were positioned at about 18 mm from the fracture, which occurred in the same region and with a very similar profile in both A specimens. Thanks to the analysis of the strain evolution by the DIC method, it was noticed that, in the first seconds of the tensile test, a greater deformation occurred near the main voids than in the fracture zone.

More interesting results are obtained in the case of the specimens with 25% straight infill. In specimen C_1 the fracture area was just 1.8 mm far from the tertiary void, while the major deformation band corresponded to the location of the secondary porosity. In specimen C_2, only the match between the position of the secondary flaw and the location of the largest deformation band was identified. Unlike A specimens, C_1 and C_2 samples did not break at the same point (Figure 10).

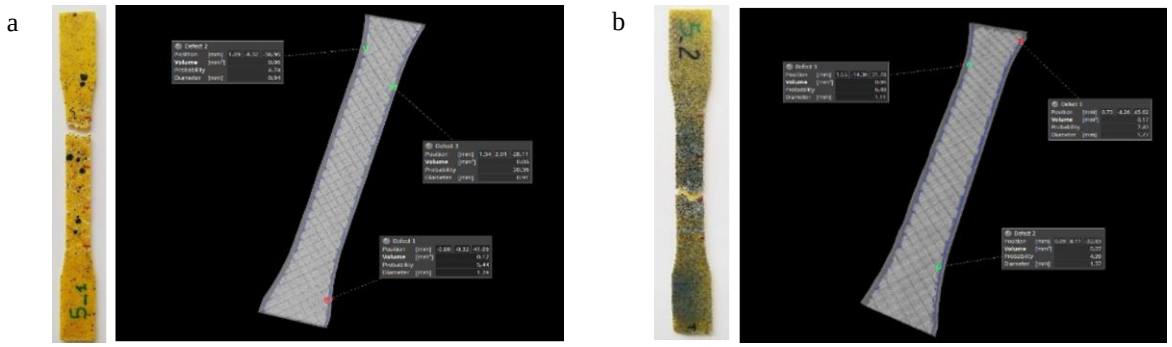

Fig. 10. Comparison of fracture region and position of the main voids in specimen C_1 (a) and specimen C_2 (b).

The results obtained for specimens with 50% infill (specimens B and D) are less consistent than the previous ones. In the case of B specimens, the match between the fracture location and the position of one of the three voids was found for only one sample. Better matching was determined for the location of the major deformation band.

In the case of D_1 and D_2 samples, the tensile fracture occurred very close to the tertiary void (Fig. 11), while the band of high strain was near the primary void.

For all E specimens, the location of the high deformation band matched the position of one of the major voids. No proximity of the three main pores to the failure zone was detected for specimens E_3 and D_3. However, for both samples, a group of smaller voids was located close to the fracture. This result strengthens the abovementioned assumption that the coalescence of smaller pores during the tensile test may overcome the importance of a larger initial void in leading to failure.

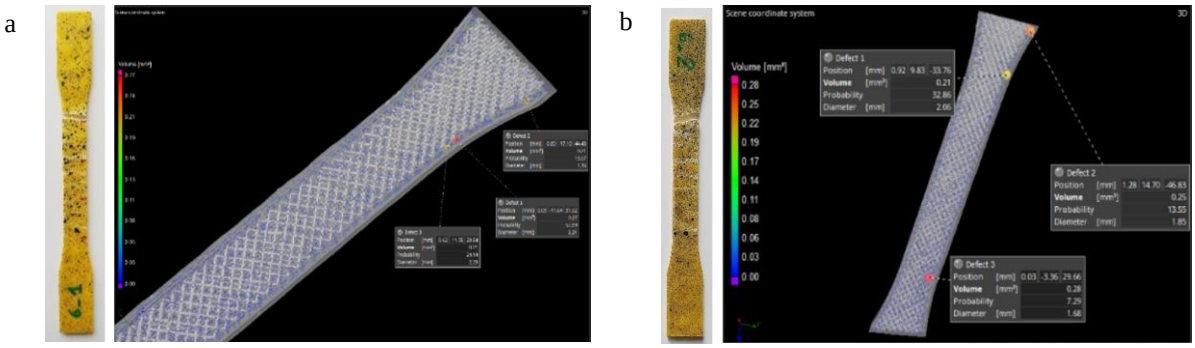

Fig. 11. Comparison of fracture region and position of the main voids in specimen D_1 (a) and specimen D_2 (b).

4. Summary and Conclusions

In this paper, an experimental campaign was conducted on 3d printed ABS specimens to associate the presence of internal voids with the tensile strength. Fourteen tensile specimens were printed varying the infill strategy and percentage. Before testing, all samples were inspected by X-ray tomography to identify and measure the main internal voids. Tensile tests were recorded by a digital camera and the digital image correlation method was applied to

distinguish the local strain in the specimen.

The results of the study, which combine the porosity analysis and the mechanical characterization, show that 25%-infill specimens with lower porosity have better tensile strength, so a relation exists between the internal voids in the material and its ultimate resistance. For 25% infill, no difference was recognized in specimens with octagonal and straight infill strategies. These specimens showed similar porosity percentages and comparable tensile strength.

On the contrary, for most of the specimens with 50% infill and 100% infill, a clear relation between the porosity content and the tensile strength could not be assessed. However, specimens with 50% octagonal infill showed a higher average value of the tensile strength if compared to sample with 50% straight infill.

Using the results of the DIC analysis, for many specimens a match was found between the position of one main void and the location of the fracture or the location of the major deformation band.

This work points out the importance of the analysis of internal flaws in 3d printed parts to detect the areas of part failure. When in-situ monitoring of the 3d printing process is not applied or available, CT data should be used to predict the resistance of critical products preventing unexpected failures. Further experimental activities should be carried out to extend this preliminary study with the aim of collecting more data to strengthen the statistical significance of the presented results.

References

[1] Calignano F, Manfredi D, Ambrosio EP, Biamino S, Lombardi M, Atzeni E, Salmi A, Minetola P, Iuliano L, Fino P. Overview on additive manufacturing technologies, Proc. IEEE 105(4) (2017) 593-612.

[2] Rinaldi M, Ghidini T, Cecchini F, Brandao A, Nanni F. Additive layer manufacturing of poly (ether ether ketone) via FDM, Composites Part B: Engineering 145 (2018) 162-172.

[3] Zekavat AR, Jansson A, Larsson J, Pejryd L. Investigating the effect of fabrication temperature on mechanical properties of fused deposition modeling parts using X-ray computed tomography, Int. J. Adv. Manuf. Technol., 100(1-4) (2019) 287-296.

[4] Chen RK, Lo TT, Chen L, Shih AJ. Nano-CT characterization of structural voids and air bubbles in fused deposition modeling for additive manufacturing, In International Manufacturing Science and Engineering Conference 56826 (2015) V001T02A071.

[5] Chin Ang K, Fai Leong K, Kai Chua C, Chandrasekaran M. Investigation of the mechanical properties and porosity relationships in fused deposition modelling-fabricated porous structures, Rapid Prototyp. J. 12(2) (2006) 100-105.

[6] Gebisa A, Lemu H. Investigating Effects of Fused-Deposition Modeling (FDM) Processing Parameters on Flexural Properties of ULTEM 9085 using Designed Experiment, Materials 11 (2018) 500.

[7] Calignano F, Lorusso M, Roppolo I, Minetola P. Investigation of the Mechanical Properties of a Carbon Fibre-Reinforced Nylon Filament for 3D Printing, Machines 8(3) 2020 52.

[8] Hsueh MH, Lai CJ, Liu KY, Chung CF, Wang SH, Pan CY, Huang WC, Hsieh CH, Zeng YS. Effects of Printing Temperature and Filling Percentage on the Mechanical Behavior of Fused Deposition Molding Technology Components for 3D Printing. Polymers. 13(17) (2021) 2910.

[9] Minetola P, Khandpur MS, Iuliano L, Calignano F, Galati M, Fontana L. In-Situ Monitoring for Open Low-Cost 3d Printing, In: Agarwal RK (eds) Recent Advances in Manufacturing Engineering and Processes. Lecture Notes in Mechanical Engineering. (2022) Springer, Singapore.

[10] Wang X, Zhao L, Fuh JYH, Lee HP. Effect of Porosity on Mechanical Properties of 3D Printed Polymers: Experiments and Micromechanical Modeling Based on X-ray Computed Tomography Analysis, Polymers 11(7) (2019) 1154.

[11] Englert, L., Dietrich, S. and Pinter, P. Investigations on printing path dependent properties of additively manufactured samples using micro computed tomography, Rapid Prototyp. J. 26(9) (2020) 1603-1614.

[12] ASTM International. ASTM E3166-20 - Standard Guide for Nondestructive Examination of Metal Additively Manufactured Aerospace Parts After Build. 2020.

[13] Jerabek, M, Major Z, Lang RW. Strain determination of polymeric materials using digital image correlation. Polymer Testing 29(3) (2010) 407-416.

[14] ASTM International. ASTM D638-14 - Standard Test Method for Tensile Properties of Plastics. 2017.